

Supplementary information

Citric juice-mediated Synthesis of Tellurium Nanoparticles with Antimicrobial and Anticancer Properties

David Medina^{1,†}, William Tien-Street^{1,2,†}, Bohan Zhang^{1,†}, Xinjing Huang^{1,†}, Ada Vernet Crua¹, Alfonso Nieto-Argüello³, Jorge L. Cholula-Díaz³, Lidia Martínez⁴, Yves Huttel⁴, María Ujué González⁵, José Miguel García-Martín⁵ and Thomas J. Webster^{1,*}

†These authors contributed equally to this paper.

¹ Department of Chemical Engineering, Northeastern University, Boston, MA 02115, USA

² Department of Bioengineering, Northeastern University, Boston, MA 02115, USA

³ School of Engineering and Sciences, Tecnológico de Monterrey, Av. Eugenio Garza Sada 2501, Monterrey, NL 64849, Mexico.

⁴ Materials Science Factory. Instituto de Ciencia de Materiales de Madrid, ICMM-CSIC, Sor Juana Inés de la Cruz 3, 28049 Madrid, Spain

⁵ Instituto de Micro y Nanotecnología, IMN-CNM, CSIC (CEI UAM+CSIC), Isaac Newton 8, 28760 Tres Cantos, Spain

*Correspondence: Thomas J. Webster

Department of Chemical Engineering, Northeastern University,

313 Snell Engineering Center, 360 Huntington Avenue, Boston, MA 02115

Tel +1 617 373 6585

Fax +1 617 373 2209; Email: th.webster@neu.edu

Synthesis of TeNPs

Color change within the solution after microwave-assisted reaction at different metallic salts concentrations for LEM-TeNPs employing lemon juice extract (Figure S1). Identical results were found when the other extracts –orange and lime- were employed. The coloration appeared a few seconds after the heating cycle.

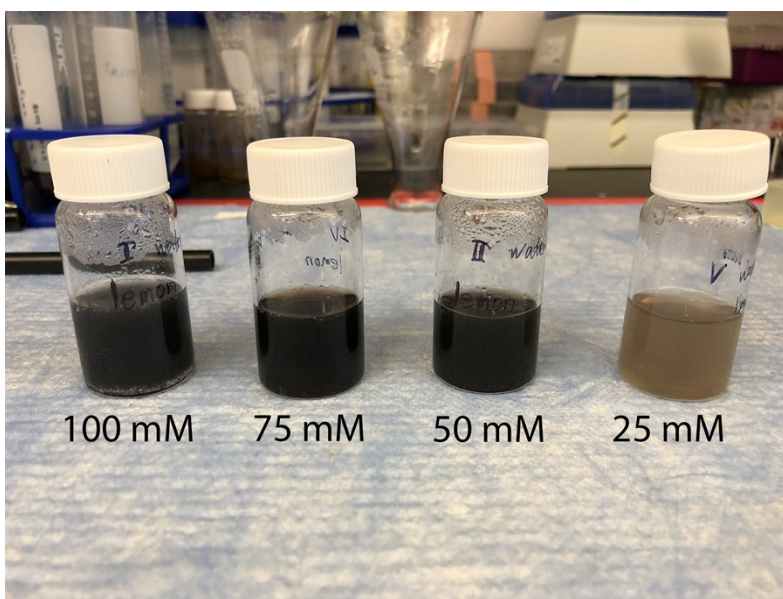


Figure S1. Coloration of reaction mixture after microwave-assisted synthetic approaches for different Te-precursor solution concentrations. From left to right, a decrease of the metallic salt (sodium tellurite) concentration is translated in a brighten of the black coloration within the solution.

TEM characterization of TeNPs

OR-, LEM- and LIM-TeNPs were prepared using a microwave-assisted method with a decrease of the Te-precursor solution concentration from 100 to 25 mM, leading to some changes in the morphology and aggregation of the structures, with the presence of clusters at high concentrations (Figures S2, S3 and S4).

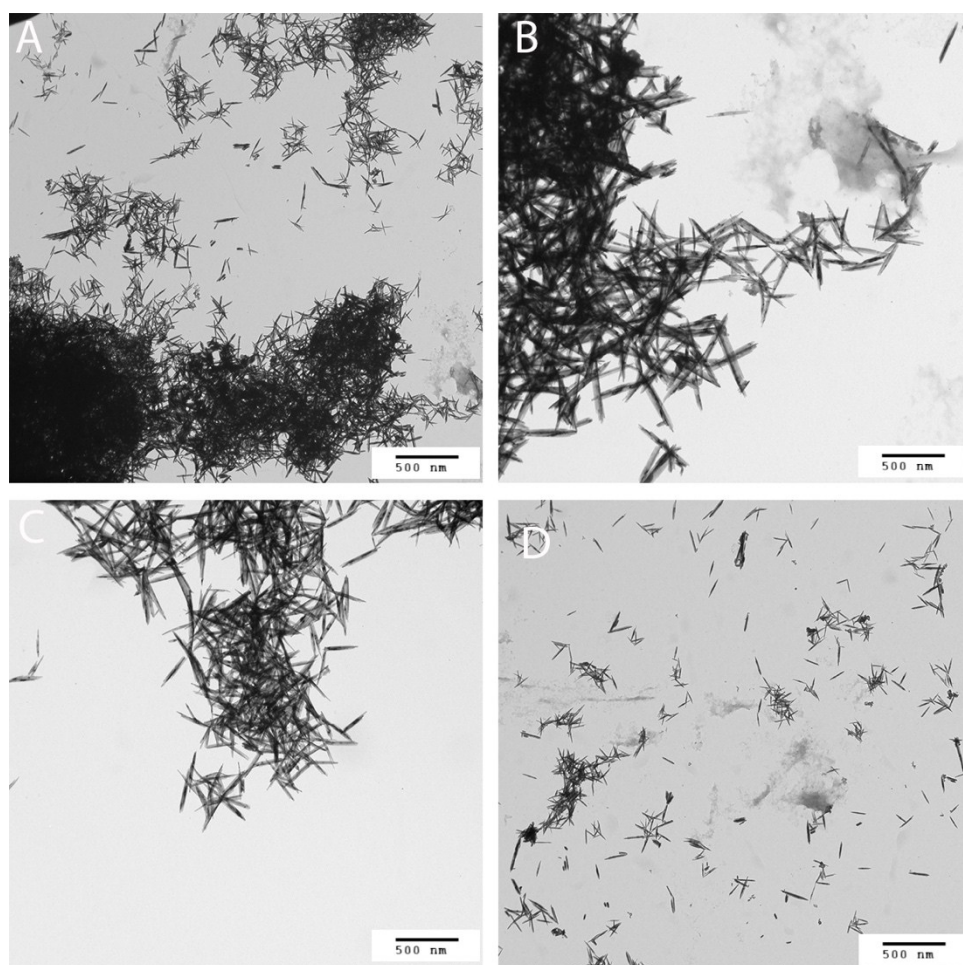


Figure S2. TEM characterization of OR-TeNPs when 100 mM (A), 75 mM (B), 50 mM (C) and 25 mM (D) Te-precursor solution concentration was used.

For OR-TeNPs, needle-like nanostructures were found to generate clusters at high concentrations, with less presence of the aggregates when the concentration of Te-precursor solution was decreased, while the morphology was the same for all the samples (Figure S2).

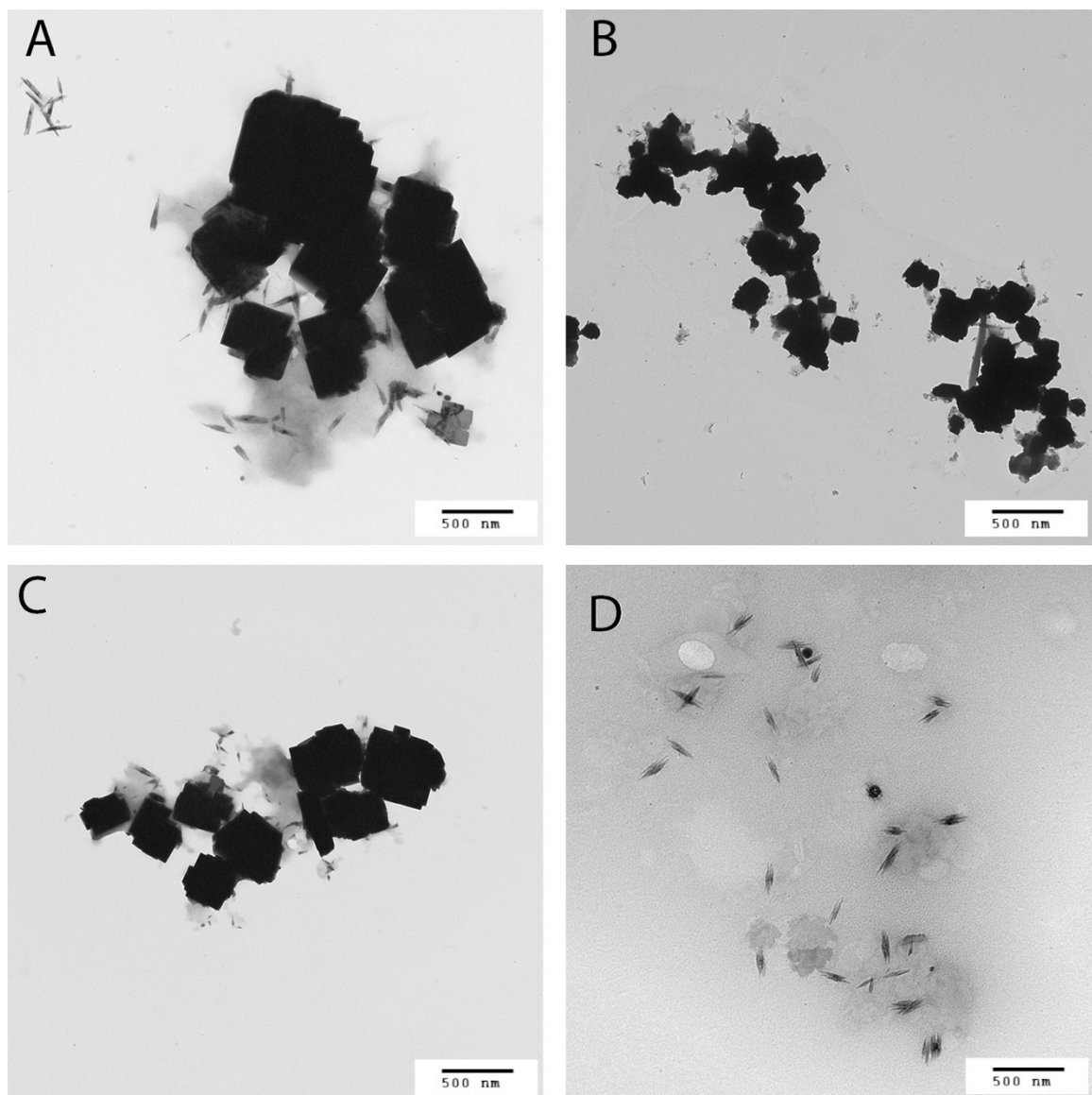


Figure S3. TEM characterization of LEM-TeNPs when 100 mM (A), 75 mM (B), 50 mM (C) and 25 mM (D) Te-precursor solution concentration was used.

For LIM-TeNPs, cubic-shaped nanostructures were found, with a size-metallic salt concentration dependence (Figure S3). For the lowest concentration, no cubic structures were found, while some nanorod-like structures were observed.

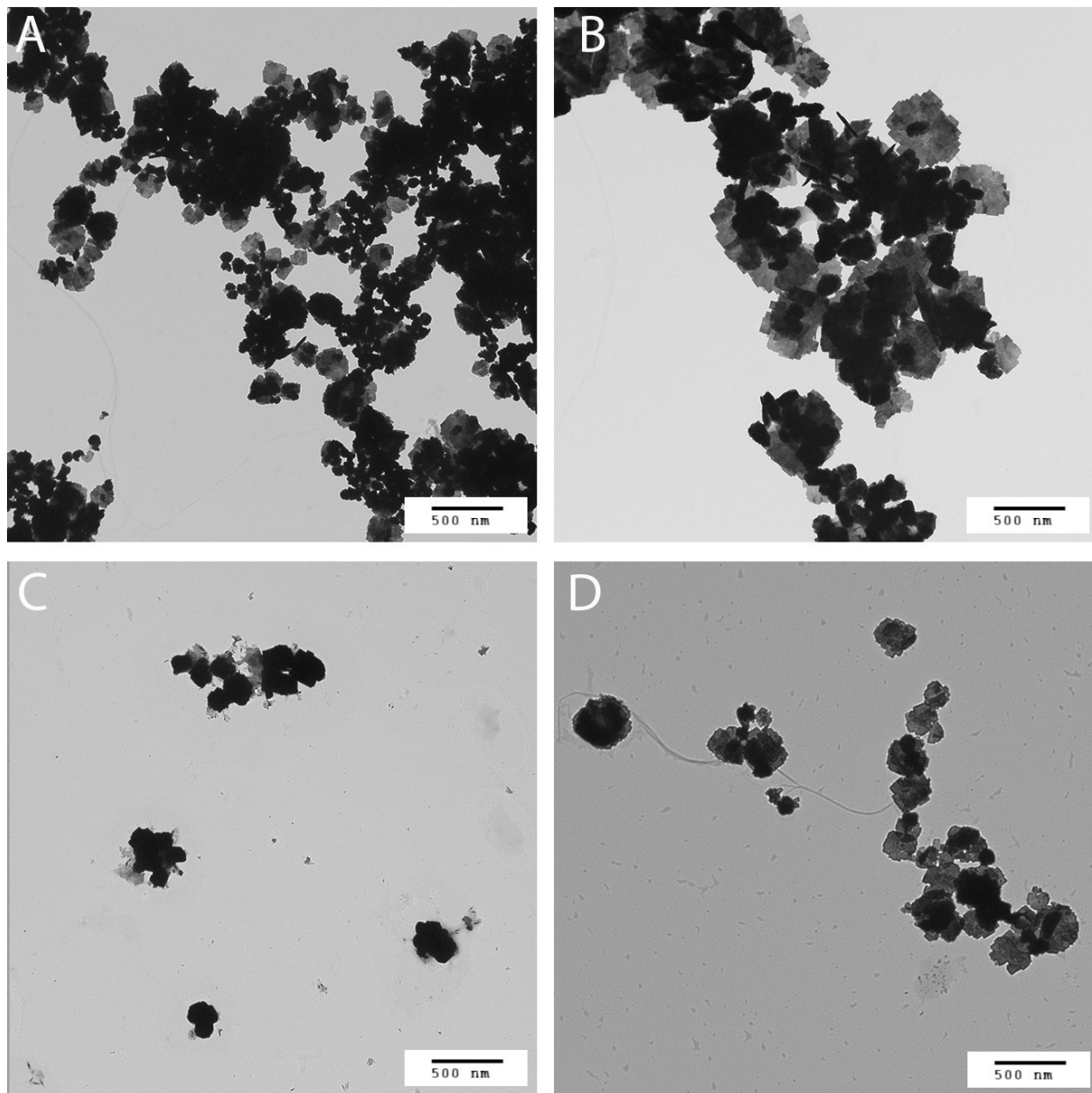


Figure S4. TEM characterization of LIM-TeNPs when 100 mM (A), 75 mM (B), 50 mM (C) and 25 mM (D) Te-precursor solution concentration was used.

For LIM-TeNPs, cubic-shaped nanostructures were found, with some agglomerates for the highest Te-precursor solution concentrations (Figure S4). The agglomeration decreases when the metallic salt concentration is lowered. The presence of some nanorods together with the cubic-like structures were noticed.

EDX characterization

Different areas of each sample were analyzed in order to assess the substances present in the nanostructures. The characterization confirmed that the electron-dense nanoparticles were composed of tellurium as proven by the presence of specific tellurium peaks in all samples. For OR-TeNPs (Figure S5), the analysis indicated the presence a single kind of nanostructures, Te nanorods, surrounded by a matrix composed mainly of carbon, oxygen, sodium and potassium.

As the ratio between the oxygen content and the carbon content is almost the same in area 1, with lots of nanorods, and in area 2, with mainly organic coating, we can infer that the nanorods are mainly composed of metallic Te. For LEM- and LIM-TeNPs (Figures S6 and S7, respectively), analysis of the different positions corroborated the presence of two tellurium structures, small tellurium nanoparticles, visible in the back-scattered electrons SEM images, and bigger cubic-shape crystals. In all samples, significant oxygen, carbon and sodium peaks were also identified, indicating the presence of a matrix embedding the nanostructures coming from the citric extract and the salt used in the synthesis process. Focusing our attention in Fig. S6 corresponding to LEM-Te NPs, the ratio oxygen(atomic%)/carbon(atomic %) in Spot 1, on top of a big cubic-shape crystal, is four times higher than that in Area 2 without big crystal, which indicates that the big crystal contains a significant amount of oxygen. Thus, such a higher content of oxygen suggests

partial oxidation of the tellurium core, in agreement with the XRD patterns (Figure 3 in the main manuscript). A similar case is deduced from Figure S7 corresponding to LIM-Te NPs. Finally, potassium, magnesium and calcium species were also found in all the spectra and it has been hypothesized that their presence may be derived from the orange, lemon and lime themselves, as well as from the metallic salt (sodium-containing tellurite). As described in the literature, citric juices contain a good amount of potassium¹, being the metal in highest content, with values between 15 and 300 mg/L. The detected silicon amount came from the use of Si substrates for the sample deposition.

OR-Te NPs

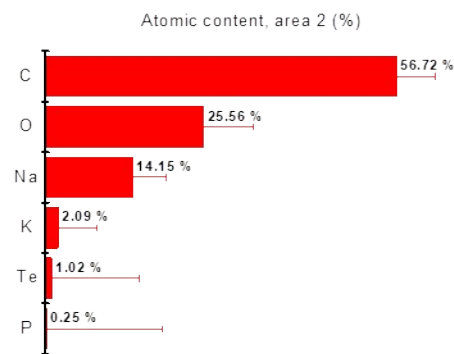
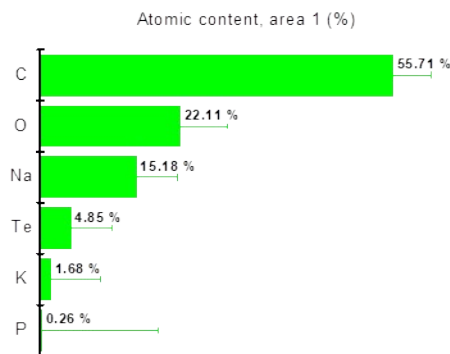
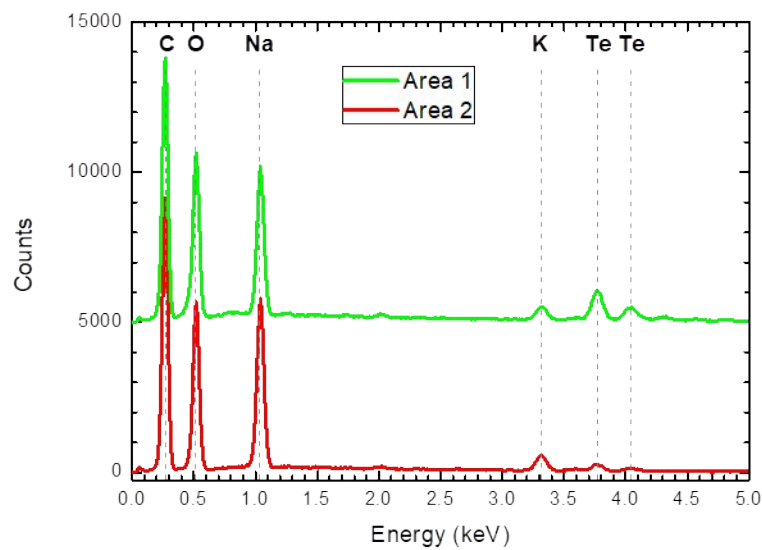
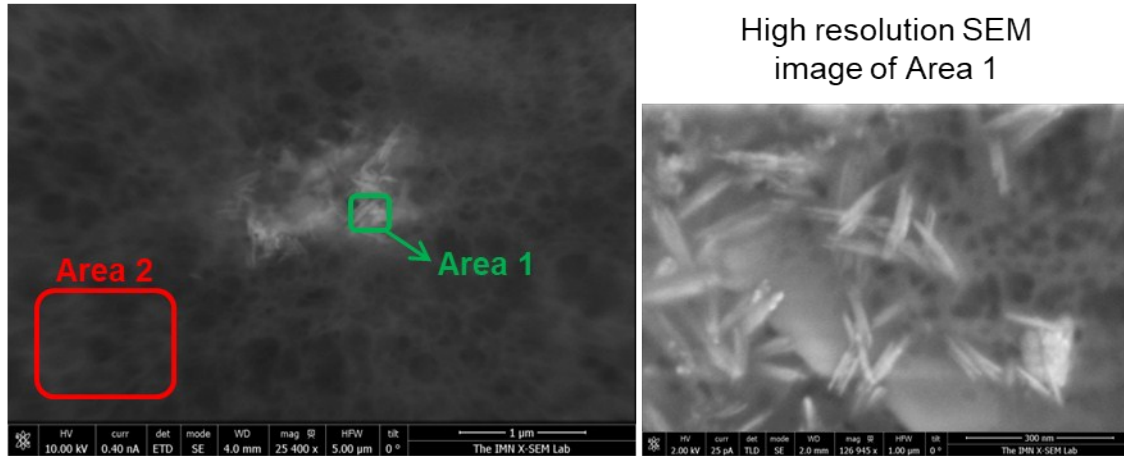


Figure S5. EDX characterization of OR-TeNPs, showing the presence of tellurium within the sample, as well as carbon, oxygen and sodium. The spectra were taken in different zones: Area 1 corresponds to the tellurium nanorods embedded in an organic matrix, and Area 2 corresponds to the surrounding matrix with some buried nanostructures not observed in the image (some tellurium is also detected there).

LEM-Te NPs

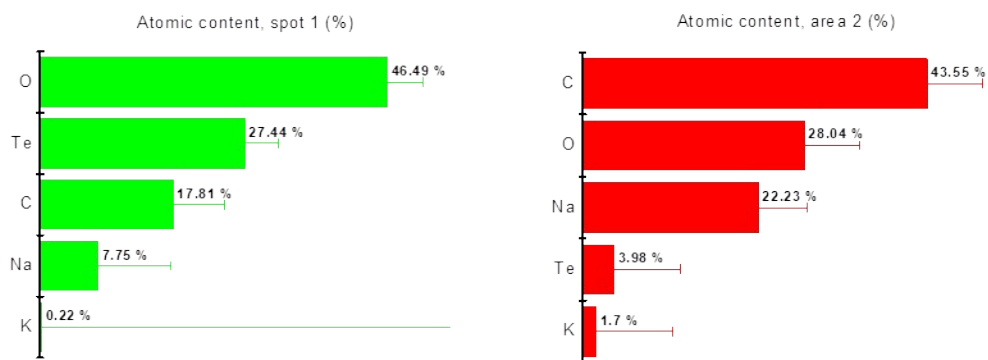
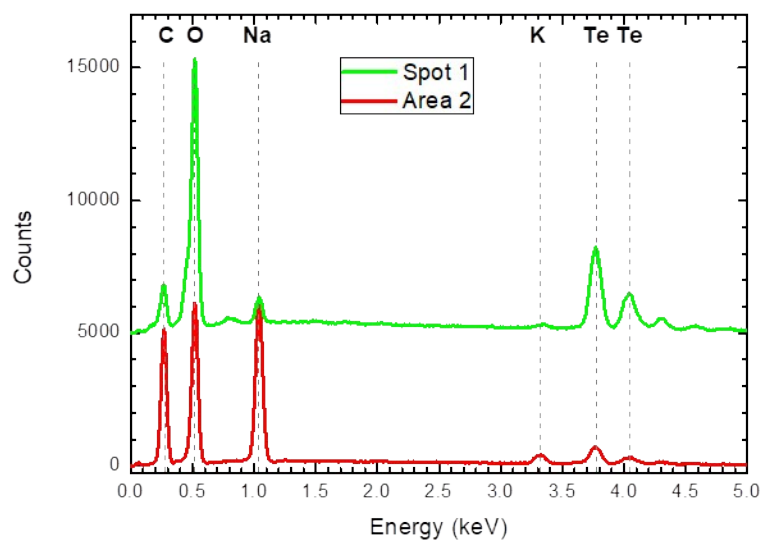
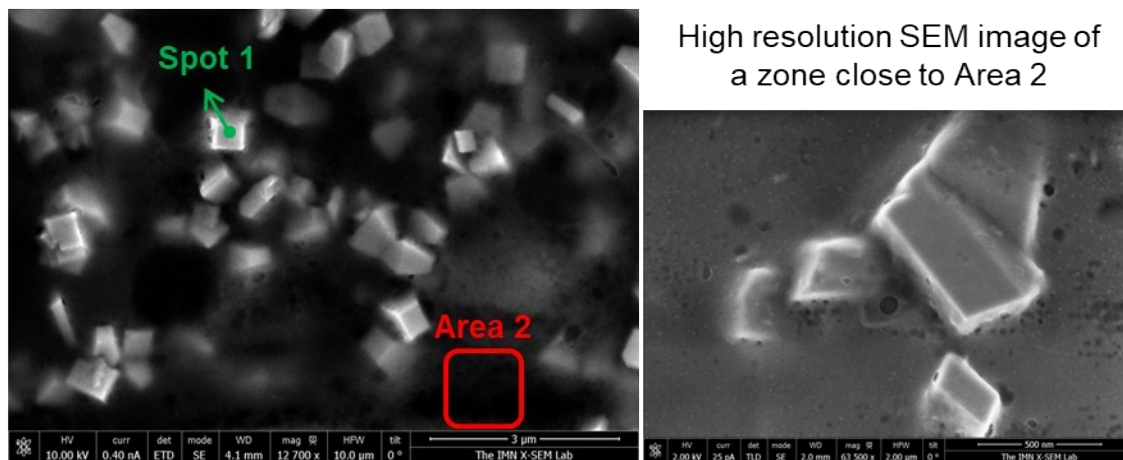


Figure S6. EDX characterization of LEM-TeNPs, showing the presence of tellurium within the sample, as well as carbon, oxygen and sodium. The spectra were taken in different zones: Spot 1 corresponds to one of the big tellurium crystals found in the sample and Area 2 corresponds to the surrounding organic matter, where the small dispersed nanoparticles are confirmed to be made of tellurium.

LIM-Te NPs

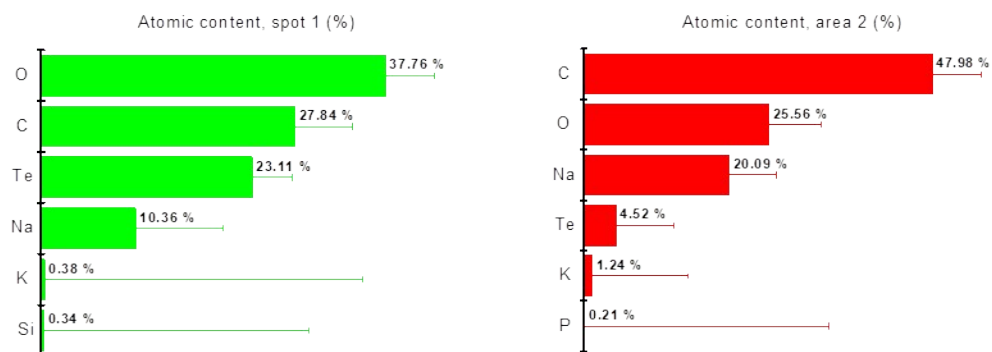
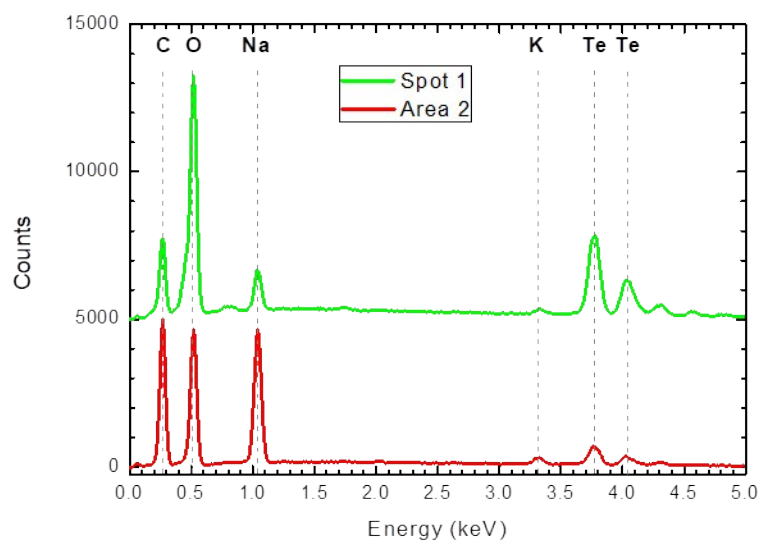
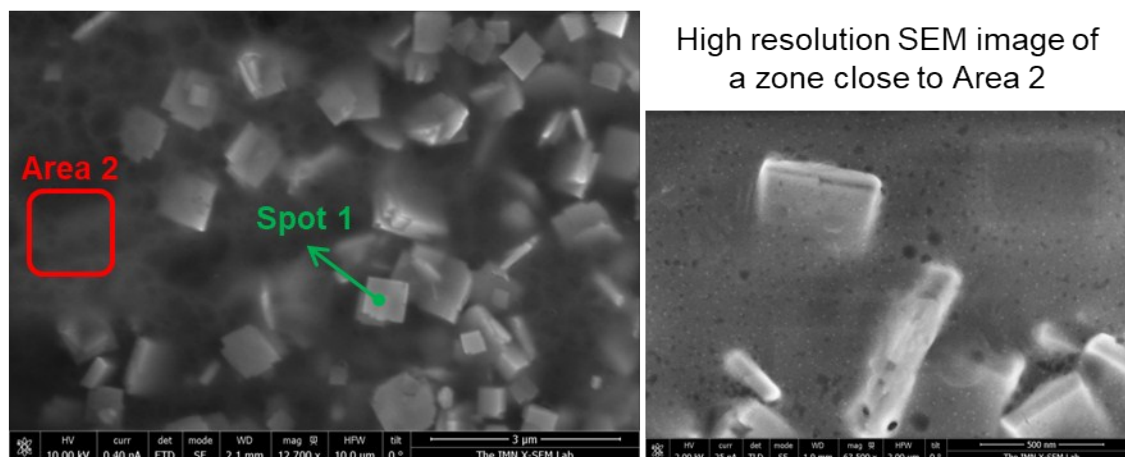


Figure S7. EDX characterization of LIM-TeNPs, showing the presence of tellurium within the sample, as well as carbon, oxygen and sodium. The spectra were taken in different zones: Spot 1 corresponds to one of the cubic tellurium crystals found in the sample and Area 2 corresponds to the surrounding organic matter, where the small dispersed nanoparticles are confirmed to be made of tellurium.

XRD characterization

XRD patterns are shown in Figure 3 in the main manuscript. The lattice parameters calculated for OR-TeNPs and the orthorhombic LEM-TeNPs and LIM-TeNPs are also reported in Table S1.

*Table S1. Lattice parameters calculated for Orange-TeNPs (*h*-Te) and, Lemon-TeNPs and Lime-TeNPs (β -TeO₂)*

Sample	<i>a</i> / Å	<i>b</i> / Å	<i>c</i> / Å
OR-TeNPs	4.476	4.476	5.856
<i>h</i> -Te ²	4.456	4.456	5.921
LEM-TeNPs	12.019	5.419	5.546
LIM-TeNPs	12.045	5.434	5.547
β -TeO ₂ ³	12.035	5.464	5.607

XPS analysis

Figure 4 in the main manuscript presents the wide energy range scan of the Te nanoparticles obtained from the orange, lime and lemon juices using XPS analysis. Quantification is reported in Table S2. A comparison of the three samples evidenced that the higher Te concentration was detected in the lemon dispersion, which doubled the orange one.

Table S2. Composition of the samples extracted from the wide energy range scans displayed in Figure S8.

	Composition at%				
	C	N	Na	O	Te
OR-TeNPs	59.2	1.7	1.0	37.7	0.4
LIM-TeNPs	65.0	1.1	0.6	32.6	0.6
LEM-TeNPs	62.5	1.1	1.2	34.4	0.8

Detailed analysis of the core level peaks enabled the observation of certain differences between the samples. Figure S8 (left) presents the Te 3d core level peak of the samples. Two components are present in the Te 3d; the first component at 573 ± 0.1 eV corresponds to the metallic component of Te $3d_{5/2}$ and the other component at 576 ± 0.2 eV, corresponds to the oxidized component^{4,5}. . By having a look to the proportion between the metallic and the oxidized components (Table S3), LEM-TeNPs - the samples with higher metallic Te proportion – only presented a 6 at% of Te oxidized, whereas the amount of oxidized Te is 18 at% in OR-TeNPs. The difference between these results and those obtained with the other techniques (EDX, XRD) is due to the inherent characteristics of the technique: XPS is a surface analysis technique where the average depth of analysis for a XPS measurement is only a few nm, much smaller than the penetration depth in the measurements by EDX and XRD.

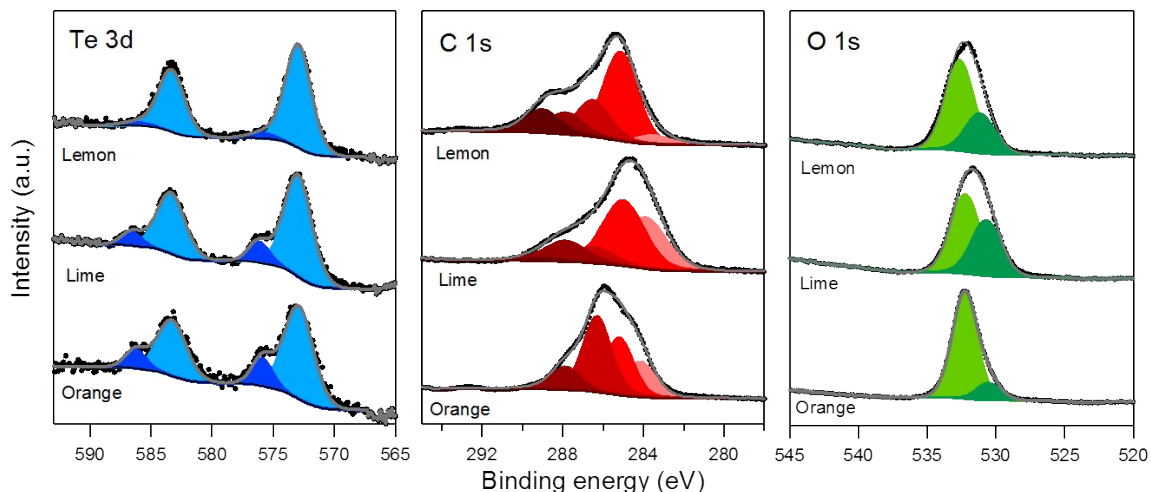


Figure S8. XPS Core level spectra of Te 3d (left), C 1s (center) and O 1s (right) of OR-, LEM- and LIM-TeNPs, respectively.

Besides, the analysis of the C 1s core level spectra of the samples revealed significant differences between the samples (Figure S8 (center)). Five components were used for the fitting, all of them were forced to have the same full width at half maximum (FWHM). These components corresponded to C-C/C-H bonds at 285 ± 0.2 eV; C-O / C-N bonds at 286.3 ± 0.2 eV; C=O bonds at 288.1 ± 0.2 eV and O-C=O bonds at 289 ± 0.2 eV. These four components are typical from organic compounds⁶. The fifth component that appeared at a lower binding energy (284 ± 0.2 eV) can be attributed to carbon in the sp^2 configuration⁷. The relative intensity of each component varies depending on the sample. Table S3 displays the proportion of each component of the C 1s and O 1s. OR-TeNPs – the one with the highest amount of oxygen – is the only sample in which the main component of the C 1s is not the C-C bond, and the C-O contribution is the most abundant. In the three samples, the C=O contribution is similar (around 13 at%). Only in the lemon sample, the O-C=O contribution is representative and reaches 13 at%.

The O 1s core level of the samples can be fitted into two components, one at 532.3 ± 0.2 eV and another less intense at 530.8 ± 0.2 eV (Figure S8 (right)). The first component is in the energy range characteristic of carbon-oxygen bonds in organic compounds⁶. The second component is close to the energy range of Te oxide [NIST database <https://srdata.nist.gov/xps/>] although by having a look to the amount of Te oxide of each sample (Table S3), it is clear that there are also other contributions to this component. The elements present in small amounts (i.e., N, Na, Cu) can also contribute to this component when bonded to oxygen.

Table S3. Components used for the fitting of the C 1s and O 1s core levels.

	Te	TeO _x	C-C	C-O	C=O	O-C=O	sp ²	O1	O2
OR-TeNPs	82	18	30	41	12	0	17	83	17
LIM-TeNPs	86	14	42	11	14	2	31	59	41
LEM-TeNPs	94	6	49	21	13	13	5	70	30

Stability analysis

In order to verify the stability of the citrics-mediated Te nanoparticles synthesized using a metal precursor concentration of 50 mM, TEM imaging on the samples after 60 days of synthesis were carried out (Figure S9). In general, it is evident that the samples kept their original morphologies and features. For example, the 60-days old OR-TeNPs sample is composed of partial agglomerated thin nanoneedles (50-200 nm length and 2-15 nm wide), as seen in Figure S9A. These features are in accordance with the freshly synthesized OR-TeNPs sample (Figures 1A in main manuscript and S2C). In the case of 60-days old LEM- and LIM-TeNPs samples, agglomerated nanocubes with

100-200 nm in length were observed (Figures S9B and S9D, respectively), which is in agreement with their corresponding initial samples (Figures 1B and 1C in the main manuscript, respectively).

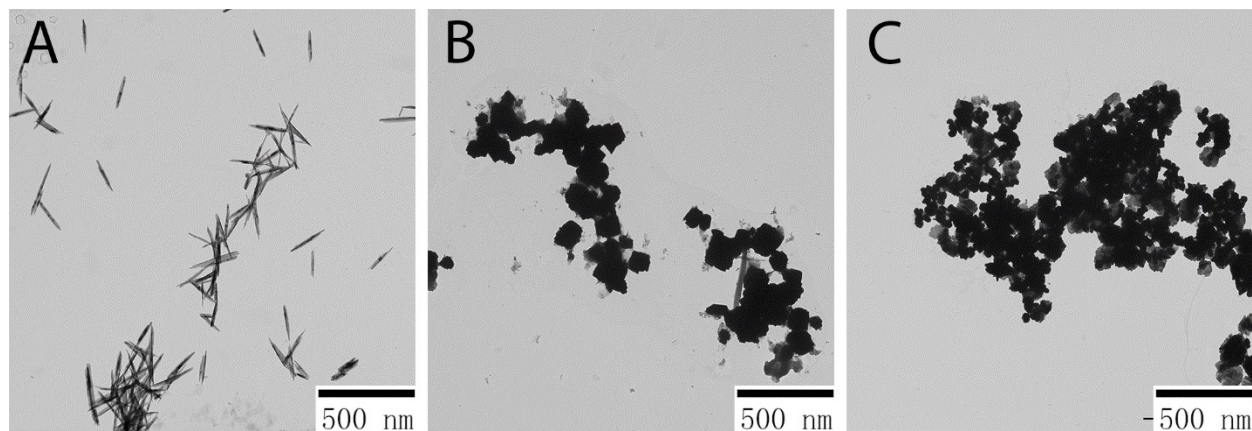


Figure S9. TEM images of OR- (A), LEM- (B) and LIM- (C) TeNPs after 60 days of synthesis. The samples were synthesized using a Te precursor concentration of 50 mM.

The stability analysis through the measurement of the Z-potential of the freshly synthesized and 60-days old Te-based nanoparticle colloids were also carried out. In general, a colloid or suspension is considered stable if the Z -potential is above a critical value of ± 30 mV⁸. Given the measured Z -potential values for the colloids OR-, LEM- and LIM-TeNPs (freshly and 60-days old samples, see Table S4), they can be considered stable.

Table S4. Zeta-potential values for freshly and 60-days old OR-, LEM- and LIM-TeNPs. The pH of the colloids were 7.0 ± 0.2

Type of NP	Z-potential (mV)	
	As-synthesized	60 days-old
OR-TeNPs	-27.06 ± 0.28	-29.11 ± 0.09
LEM-TeNPs	-23.66 ± 0.98	-26.12 ± 1.01
LIM-TeNPs	-30.18 ± 1.84	-28.39 ± 2.2

Antimicrobial activity of TeNPs

The antimicrobial activity of the different Te nanostructures was evaluated using 24-hours growth curve analysis, with results are displayed in Figure S10.

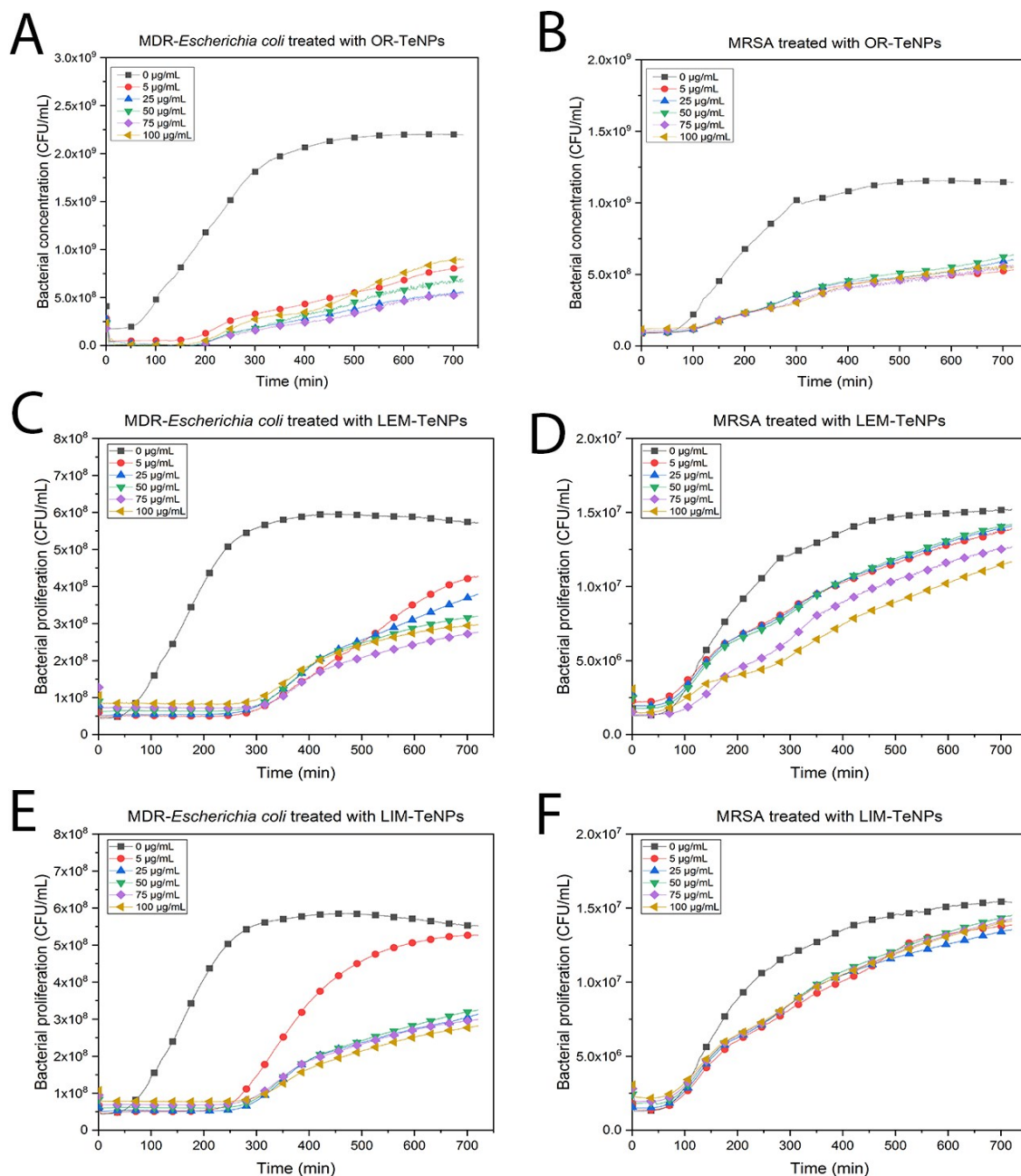


Figure S10. Citric-mediated TeNPs decrease the growth of *Escherichia coli* (A, C, E) and *Staphylococcus aureus* (B, D, F). Growth of a 10^6 CFU mL⁻¹ suspension of *Escherichia coli* (MDR-*E. coli*) and *Staphylococcus aureus* (MRSA) over 24 h in presence of different concentrations of tellurium nanoparticles. Data = mean +/- SEM, N = 3.

The parameters in the Gompertz equation were calculated and plotted for analysis for the three Te nanosystems. The parameter A represents the maximum specific growth of the bacteria under experimental conditions. Upon analysis of this parameter, it was found that a larger Te nanoparticle concentration led to lower asymptotic absorbance values (Figure S11A and S11B). The antibacterial activity was especially noticeable in the case of MDR *E. coli* (Figure S11A). The bigger decay in asymptotic absorbance was found in the treatment with these bacteria. In general, the OR-TeNPs displayed an antibacterial effect for both Gram-positive and -negative bacteria.

The maximum value of growth speed by the bacteria was analyzed using the parameter μ (Figures S11C and S11D). The plots demonstrated that larger TeNP concentrations resulted in lower maximum values reached for the bacteria; again, this was especially visible in the experiments with MDR *Escherichia coli* (Figure S11C). Finally, the parameter λ that represents the lag time in the bacterial growth under experimental conditions was analyzed, and results are shown in Figure S11E and S11F. Results showed that a higher TeNP concentration led to a shorter lag phase for bacterial growth. This was especially visible in the experiments with MDR *Escherichia coli* (Figure S11E), however, this trend was less obvious in the experiments with MRSA (Figure S11F). Since the lag phase refers to the point where bacteria are adapting themselves to the growth conditions offered by the media with nanoparticles, the delay may mean that the nanoparticles delay the maturing of bacteria, which are then unable to proliferate the way they should. The presence of nanoparticles may affect the bacterial growth cycle through the synthesis of RNA, enzymes or other molecules involved in this phase, which will need to be assessed in future studies.

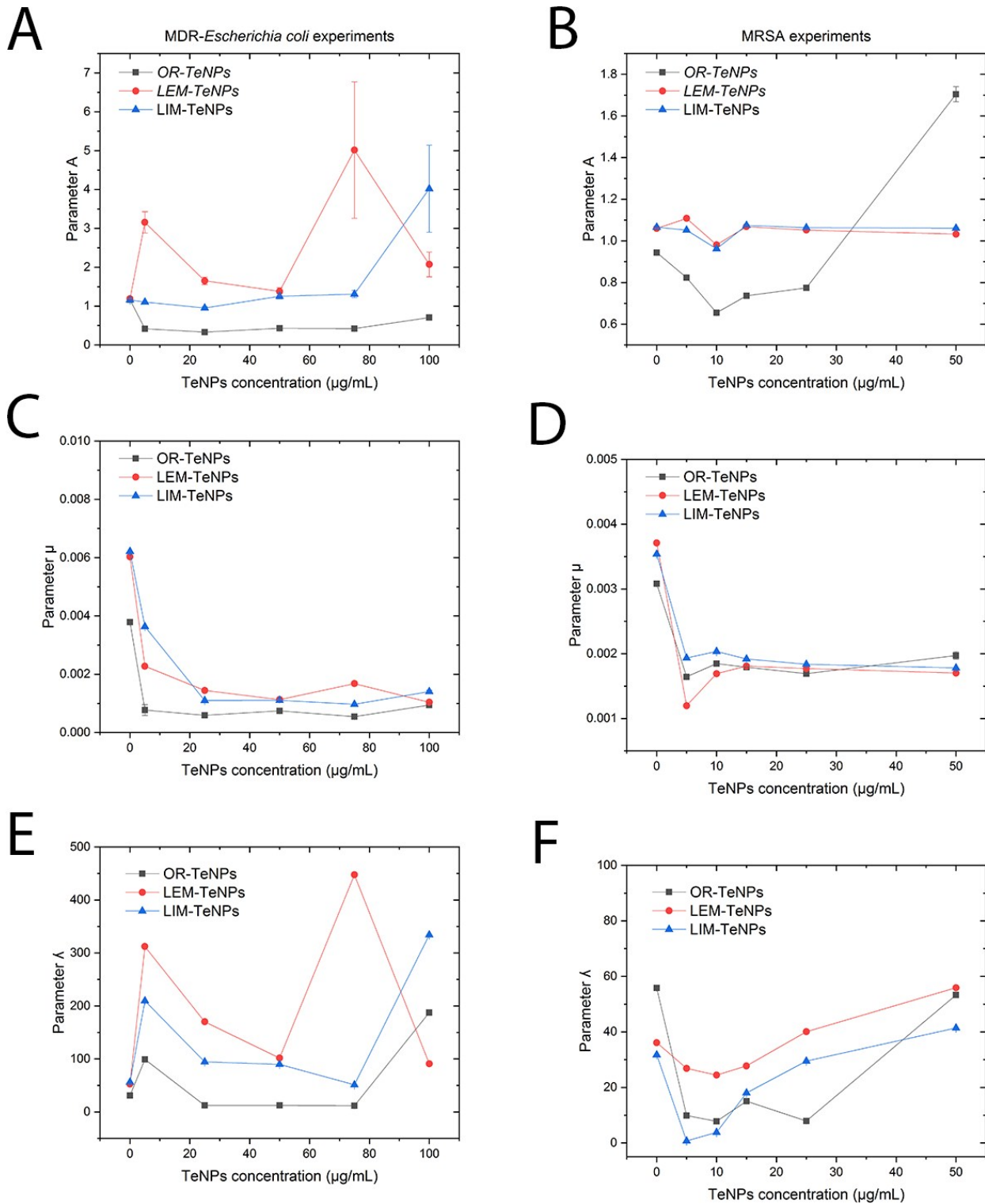


Figure S11. Gompertz parameters evaluation. The Gompertz parameters have been evaluated for the different nanoparticles (OR-, LEM- and LIM-TeNPs) in experiments with *Escherichia coli* (A,C,E) and *Staphylococcus aureus* (B,D,F). Data = mean +/- SEM.

References

- (1) D'Elia, L.; Barba, G.; Cappuccio, F. P.; Strazzullo, P. Potassium Intake, Stroke, and Cardiovascular Disease. *J. Am. Coll. Cardiol.* **2011**, *57* (10), 1210–1219.
<https://doi.org/10.1016/j.jacc.2010.09.070>.
- (2) Adenis, C.; Langer, V.; Lindqvist, O. Reinvestigation of the Structure of Tellurium. *Acta Crystallogr. Sect. C Cryst. Struct. Commun.* **1989**, *45* (6), 941–942.
<https://doi.org/10.1107/S0108270188014453>.
- (3) Beyer, H. Verfeinerung Der Kristallstruktur von Tellurit, Dem Rhomischen TeO₂. *Zeitschrift fur Krist.* **1967**, *124*, 228–237.
- (4) Beamson, G.; Briggs, D. High Resolution XPS of Organic Polymers: The Scienta ESCA300 Database. *J. Chem. Educ.* **1993**, *70* (1), A25.
<https://doi.org/10.1021/ed070pA25.5>.
- (5) Nevshupa, R.; Martínez, L.; Álvarez, L.; López, M. F.; Huttel, Y.; Méndez, J.; Román, E. Influence of Thermal Ageing on Surface Degradation of Ethylene-Propylene-Diene Elastomer. *J. Appl. Polym. Sci.* **2011**, *119* (1), 242–251.
<https://doi.org/10.1002/app.32519>.
- (6) Briggs, D. Handbook of X-Ray Photoelectron Spectroscopy C. D. Wanger, W. M. Riggs, L. E. Davis, J. F. Moulder and G. E. Muilenberg Perkin-Elmer Corp., Physical Electronics Division, Eden Prairie, Minnesota, USA, 1979. 190 Pp. \$195. *Surf. Interface Anal.* **1981**, *3* (4), v–v. <https://doi.org/10.1002/sia.740030412>.
- (7) Silva, R. R.; Mejia, H. A. G.; Ribeiro, S. J. L.; Shrestha, L. K.; Ariga, K.; Oliveira Jr., O. N.; Camargo, V. R.; Maia, L. J. Q.; Araújo, C. B.; Silva, R. R.; et al. Facile Synthesis of Tellurium Nanowires and Study of Their Third-Order Nonlinear Optical Properties. *J. Braz. Chem. Soc.* **2016**, *28* (1), 58–67. <https://doi.org/10.5935/0103-5053.20160145>.

- (8) Liu, J.; Liang, C.; Zhu, X.; Lin, Y.; Zhang, H.; Wu, S. Understanding the Solvent Molecules Induced Spontaneous Growth of Uncapped Tellurium Nanoparticles. *Sci. Rep.* **2016**, *6*, 32631. <https://doi.org/10.1038/srep32631>.